Electronic structure of charge-ordered Fe_3O_4 from calculated optical, megneto-optical Kerr effect, and O K-edge x-ray absorption spectra

I. Leonov[1], A. N. Yaresko[2], V. N. Antonov[3], and V. I. Anisimov[4]

[1] *Theoretical Physics III, Center for Electronic Correlations and Magnetism,*
Institute for Physics, University of Augsburg, Germany

[2] *Max-Planck Institute for the Physics of Complex Systems, Dresden, Germany*

[3] *Institute of Metal Physics, Vernadskii Street, 03142 Kiev, Ukraine and*

[4] *Institute of Metal Physics, Russian Academy of Science-Ural Division,*
620219 Yekaterinburg GSP-170, Russia

(Dated: February 3, 2008)

Abstract

The electronic structure of the low-temperature (LT) monoclinic magnetite, Fe_3O_4, is investigated using the local spin density approximation (LSDA) and the LSDA+U method. The self-consistent charge ordered LSDA+U solution has a pronounced [001] charge density wave character. In addition, a minor $[00\frac{1}{2}]$ modulation in the phase of the charge order (CO) also occurs. While the existence of CO is evidenced by the large difference between the occupancies of the minority spin t_{2g} states of "2+" and "3+" Fe_B cations, the total $3d$ charge disproportion is small, in accord with the valence-bond-sum analysis of structural data. Weak Fe orbital moments of $\sim 0.07\mu_B$ are obtained from relativistic calculations for the CO phase which is in good agreement with recent x-ray magnetic circular dichroism measurements. Optical, magneto-optical Kerr effect, and O K-edge x-ray absorption spectra calculated for the charge ordered LSDA+U solution are compared to corresponding LSDA spectra and to available experimental data. The reasonably good agreement between the theoretical and experimental spectra supports the relevance of the CO solution obtained for the monoclinic LT phase. The results of calculations of effective exchange coupling constants between Fe spin magnetic moments are also presented.

PACS numbers: 71.20.-b, 71.28.+d, 71.30.+h

I.   INTRODUCTION

The problem of a theoretical description of metal-insulator transitions has a challenging history of almost 70 years. It was first addressed by Verwey, de Boer, and Peierls in the late 1930's; they pointed out the extremely important role of electron-electron correlations in a partially filled d-electron band in transition metal oxides,[1,2] e.g., nickel oxide (NiO) and magnetite (Fe_3O_4). In both systems the metal-insulator transition occurs, violating the Bloch-Wilson band-insulator concept, the only one known at that time.[3,4,5,6] These earlier observations launched the long and continuing history of the field of strongly correlated electrons. In the past 70 years, much progress has been achieved from both theoretical and experimental sides in understanding strongly correlated electrons and metal-insulator transitions.[7] However, the charge ordering proposed by Verwey behind the metal-insulator transition[8,9,10] in Fe_3O_4 remains at the focus of active debate.[11,12]

Magnetite is a permanent natural magnet. Its magnetic properties have fascinated mankind for several thousand years already.[13] Comprehensive investigation of magnetite started in 1913 when the first indication of the first-order transition was obtained by a susceptibility measurement on a synthetic polycrystal.[14,15] An anomalous transition peak at $\sim$130 K was found in addition to the already known paramagnetic-to-ferrimagnetic order transition on cooling through $\sim$850 K. Electric resistivity measurements initially performed by Okamura[16] and Verwey[8] showed that this anomalous behavior of the susceptibility coincides with a sharp two orders of magnitude increase of resistivity on cooling below $\sim$120 K.[16,17] The formal valency of Fe_B cations on the octahedral B sublattice of the inverted spinel AB_2O_4 structure is noninteger (2.5+). Verwey suggested that this transition is caused by the ordering of Fe_B cations, with a simple charge arrangement of (001) planes alternately occupied by 2+ and 3+ Fe_B cations.[8,9,10] This particular (Verwey) charge order (CO) obeys the so-called Anderson criterion[18] of minimal electrostatic repulsion leading to a short range CO pattern with each tetrahedron formed by B sites being occupied by equal numbers of 2+ and 3+ cations.

However, further experiments disproved the orthorhombic Verwey CO model. These experiments have clearly established the rhombohedral distortions of the cubic unit cell first detected by Rooksby et al. from x-ray powder diffraction.[19,20] Furthermore, observations of superstructure reflections revealed half-integer satellite reflections, indexed as $(h, k, l+\frac{1}{2})$ on

the cubic unit cell, which points to a doubling of the unit cell along the c axis and shows the symmetry to be monoclinic.[21,22] The observation of monoclinic lattice symmetry was also confirmed by a single-crystal x-ray study,[23] whereas the observation of a magnetoelectric effect indicated even lower $P1$ symmetry in the low-temperature phase.[24] Although, clear evidence of the monoclinic lattice symmetry below T_V was obtained, small atomic displacements have not been fully resolved so far. The absence of a definitive, experimentally determined structure gives rise to many theoretical models proposed for the low-temperature (LT) phase of magnetite.[25] In particular, purely electronic[26,27,28,29] and electron-phonon[30,31,32] models for CO, as well as a bond dimerized ground state without charge separation,[33] have been proposed.

At room temperature Fe_3O_4 is a poor metal with an electronic resistivity of 4 mΩ cm which is considerably higher than the resistivity of simple metals (for instance, the resistivity of Cu is 1.7 $\mu\Omega$ cm). The microscopic origin of the electronic state above the Verwey transition is still unclear. Photoemission studies performed by Chainani *et al.*[34] and Park *et al.*[35] gave controversial results indicating metallic and semiconducting behavior above T_V, respectively. In accordance with Park *et al.*,[35] qualitatively similar conclusions have been derived by Schrupp *et al.*[36] and Pimenov *et al.*[37] basing on a soft x-ray photoemission study and complex conductivity measurements at terahertz/infrared frequencies, respectively.

Magnetite is a ferrimagnet with anomalous high Curie temperature of $\sim$850 K. The A-site magnetic moments are aligned antiparallel to the B-site moments. This remarkable situation of antiferromagnetic coupling between Fe_A^{3+} and $Fe_B^{2.5+}$ cations, which have d^5 and $d^{5.5}$ electron configurations in the high-spin state, respectively, should lead to a half-metallic state with integer magnetic moment of $4\mu_B$ per formula unit. This is in qualitatively good agreement with magnetization measurements, which result in a $\sim$4.1 μ_B magnetic moment per unit cell.[38,39] In contrast, spin resolved photoemission measurements show $\sim$20% suppression of the pure negative spin polarization from the half-metallic behavior obtained for Fe_3O_4 (111) films.[40] Scanning tunneling microscopy and spin-polarized photoelectron spectroscopy give only 55% of negative spin polarization at the Fermi level.[41] To explain this phenomenon two possible scenarios have been recently proposed. According to the first, Fe_3O_4 is still a half metal in the bulk, whereas surface stresses lead to unusual lattice distortions which reduce spin polarization at the Fermi level to $\sim$40%.[41,42] An alternative explanation is the formation of nonquasiparticle or incoherent states in the gap near the

Fermi level due to correlation effects.[43]

Recent bond-valence-sum analysis[44] of high-resolution neutron and x-ray powder diffraction data results in a small charge disproportion of only $0.2\,\bar{e}$ between Fe_B cations with the 2+ and 3+ formal valency.[11,45] This interpretation has been the subject of much controversy.[12,46] However, the smallness of the charge order parameter was reproduced in an electronic structure study of the refined low-temperature crystal structure using the loacl spin density approximation (LSDA)+U method.[47,48] In particular, a more complicated charge-ordering pattern inconsistent with the Verwey CO model was obtained. In addition to that, the t_{2g} occupancy self-consistently obtained in the LSDA+U calculations is strongly modulated between the Fe_B^{2+} and Fe_B^{3+} cations, yielding a distinct orbital order with an order parameter that reaches 70% of the ideal value.[47] Since no direct experimental confirmation of this charge and orbital order pattern is so far available, the interpretation of these results is still open to debate. However, this behavior seems to be universal and has recently been found in several other charge ordered mixed-valent systems.[48,49,50,51,52]

In order to further check the pertinence of the CO model obtained self-consistently in Ref. 47 we carried out a detailed theoretical study of exchange coupling constants, optical conductivity, magneto-optical (MO) Kerr effect, and x-ray absorption at the O K edge of low-temperature Fe_3O_4 and compared the results of the calculations to the available experimental data.

The paper is organized as follows. In Sec. II we discuss the low temperature crystal structure of Fe_3O_4. Section III presents computational details relevant to reproduce the calculation results. The results of electronic structure calculations obtained by the LSDA and LSDA+U methods for the low-temperature Fe_3O_4 are presented in Secs. IV and V, respectively. In Section V a charge and orbital order are also discussed and results of calculations of exchange coupling constants are presented. In Section VI we present calculated optical, magneto-optical, and O K-edge x-ray absorption spectra and compare them to corresponding experimental spectra. Finally, the results are summarized in Section VII.

II.   CRYSTAL STRUCTURE AND CHARGE ORDER

Above the Verwey transition magnetite crystallizes in the face-centered cubic (fcc) inverse spinel crystal structure with space group $Fd\bar{3}m$. The iron atoms occupy the interstitial

positions of the close-packed fcc structure formed by the oxygen atoms. According to the chemical formula of inverse spinel, AB_2O_4, there are two different iron sublattices (A and B) distinguished by the point symmetry (T_d and D_{3d}) as well as by the averaged Fe–O distance (1.876 and 2.066 Å for A and B iron sites, respectively) and the valence state of iron cations. In particular, the A sublattice is formed by Fe^{3+} cations tetrahedrally coordinated by four oxygen ions, whereas the so-called B sublattice consists of iron sites octahedrally coordinated by six oxygen ions. The octahedral B-sites are occupied by an equal number of randomly distributed 2+ and 3+ Fe cations, which results in an average valence value of 2.5+ per each Fe_B cation. The B-sublattice is highly frustrated and can be considered as a diamond lattice of Fe_B cation tetrahedra, sharing corners with each other.

One of the driving forces for formation of the charge-ordered state in mixed valent transition metal oxides is Coulomb repulsion. In particular, another key to understanding the charge-ordered structure in Fe_3O_4 is provided by the Anderson criterion for the minimum of electrostatic repulsion energy.[18] According to Anderson each tetrahedron formed by octahedral B sites of the spinel structure is occupied by two 2+ and two 3+ Fe cations in order to minimize the intersite electrostatic repulsion. Thus, within the Cc supercell of the cubic Fe_3O_4, there are ten independent cationic arrangements, whereas one of them coincides with the Verwey model.[29] However, the Verwey CO pattern has overall the lowest classical electron correlation energy.

The low-temperature structure was shown to have a $\sqrt{2}a \times \sqrt{2}a \times 2a$ supercell with space group Cc from x-ray and neutron diffraction.[11,45] However, recent structural refinement (at 90 K) was only possible in the centric monoclinic space group $P2/c$ with $\frac{a}{\sqrt{2}} \times \frac{a}{\sqrt{2}} \times 2a$ of the cubic spinel subcell and eight formula units in the primitive unit cell.[11,45] Since the refinement for the $P2/c$ space group was found to be unstable, additional $Pmca$ orthorhombic symmetry constraints were also applied. This is equivalent to averaging the true superstructure over the additional symmetry operators, i.e., each B site in the $P2/c$ unit cell is averaged over four nonequivalent subsites in the large $\sqrt{2}a \times \sqrt{2}a \times 2a$ Cc supercell. Note, however, that such an approximation is robust in the sense of smallness of any distortions from the $P2/c$ subcell to the Cc monoclinic cell (according to Ref. 45 these are of ~0.01 Å). Previous structure refinement below T_V obtained by Iizumi *et al.* resulted in a $\frac{a}{\sqrt{2}} \times \frac{a}{\sqrt{2}} \times 2a$ subcell of the Cc unit cell and imposed orthorhombic symmetry constraints on the atomic positions.[53] In particular, a refinement based on an approximation of the true crystal structure by a centric

space group $Pmca$ or polar $Pmc2_1$ was proposed. But a charge-ordered arrangement has not been identified in this refinement, although large atomic displacements of Fe and O atoms were found. This is in strong qualitative contrast to the recent structure refinement proposed by Wright *et al.* where clear evidence of CO below the transition has been found.[11,45]

According to the refinement the octahedral Fe_B sites are split into two groups with different values of the averaged Fe–O bond distances; with $B2$ and $B3$ sites being significantly smaller than $B1$ and $B4$ ($B1$-$B4$ are crystallographically independent Fe_B sites according to the notation in Refs. 11 and 45). A different averaged Fe–O bond distance is a sensitive experimental indicator of the cation charge state. Quantitative analysis of the valence state of both Fe_B groups using the bond-valence-sum (BVS) method shows that the octahedral Fe_B sites fall into two clear groups with respect to the estimated value of valence. The result is a charge disproportion of $0.2\,\bar{e}$ between large ($B1$ and $B4$) and small ($B2$ and $B3$) sites (which has been referred as the class I CO model). Another possible class of CO arises from the symmetry-averaging orthorhombic constraint. There are 32 charge-ordered models which are refered to as class II CO because large ($B1$ and $B4$) and small ($B2$ and $B3$) sites could be averaged over (3 Fe^{2+} + Fe^{3+}) and (Fe^{2+} + 3 Fe^{2+}) subsites, respectively. The symmetry averaging results in decrease of the more pronounced charge separation of $0.4\bar{e}$ in the full Cc superstructure (class II CO) down to $0.2\,\bar{e}$ in the $P2/c$ subcell. The Anderson criterion is not satisfied by any of the class I or class II CO models. This is remarkable because the Anderson criterion has been widely used in many CO models.[28,29] However, class II, as was shown from electrostatic repulsion energy estimations, appears to be more plausible than the class I arrangement.

Recently this interpretation of the refined crystal structure has been found to be controversial. The lack of atomic long-range CO and, as a result, an intermediate valence regime below the Verwey transition were proposed.[12,46] It is argued that the difference of the average Fe-O distances between compressed and expanded FeO_6 octahedra, which could be considered as a maximum limit of charge disproportionation, has the same order as the total sensitivity (including experimental errors) of the bond-valence-sum method. This remarkable controversy shows that the understanding of the system is far from satisfactory.

III. COMPUTATIONAL DETAILS

In this paper we present results of band structure calculations which have been performed for the low-temperature crystal structure of Fe_3O_4 recently refined at 90 K.[11,45] The refined cell parameters used in calculations are $a = 5.94437$ Å, $b = 5.92471$ Å, $c = 16.77512$ Å, and $\beta = 90.236°$. The monoclinic $P2/c$ unit cell contains eight formula units. There are eight different types of iron atom sites: two tetrahedrally coordinated A sites and six B sites octahedrally coordinated by six O atoms.

The electronic structure of magnetite was calculated self-consistently using the local-spin-density approximation and LSDA+U approach[54,55] with the linear muffin-tin orbitals (LMTO) method in the atomic-sphere approximation.[56] The radii of the muffin-tin spheres were taken as $R_{Fe}= 2.125$ a.u. and $R_O= 2.0$ a.u. Fifteen kinds of empty spheres were introduced to fill up the interatomic space. As was shown in Ref. 57, weak spin-orbit coupling does not appreciably affect the band structure of Fe_3O_4. We neglect it for simplicity in Secs. IV and V. Optical, magneto-optical (MO), and x-ray absorption spectra (XAS) for the $P2/c$ model of the LT phase of Fe_3O_4 were calculated taking into account the spin-orbit coupling using the spin-polarized relativistic LMTO method.[58] In order to calculate O K-edge XAS spectra and the absorption parts of the optical conductivity in a wide energy range Fe $4f$ and O $3d$ states were included into the LMTO basis set. The dispersive parts of the conductivity were calculated using the Kramers-Kronig relations. XAS spectra were calculated in the dipole approximation neglecting relaxation effects caused by the O $1s$ core hole. A detailed description of the formalism for the calculations of MO and x-ray absorption spectra and corresponding matrix elements using the relativistic LMTO method can be found in Refs. 57,59,60 and references therein.

IV. LSDA BAND STRUCTURE

Figure 1 shows the total density of states (DOS) and band structure of Fe_3O_4 obtained from the LSDA calculations. Interestingly, the crystal structure distortion taken explicitly in the monoclinic phase does not strongly affect the electronic structure of Fe_3O_4. In particular, the calculation results agree well with previous band structure calculations for the cubic phase.[61,62] Thus, the LSDA gives a uniform half-metallic ferrimagnetic solution with partially
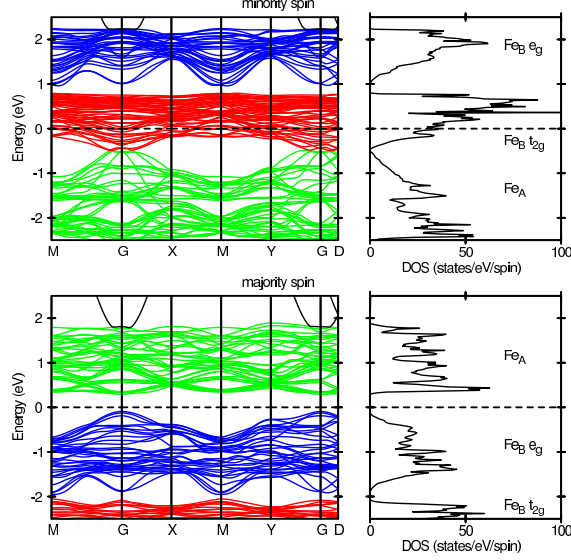
FIG. 1: (Color online) Total density of states and band structure of the $P2/c$ phase of Fe_3O_4 self-consistently obtained using the LSDA method. The Fermi level is shown by dotted lines. The energy bands predominantly originating from the Fe_A $3d$ states are shown in light gray (green) color, whereas Fe_B t_{2g} and e_g bands are in dark gray (red) and gray (blue), respectively. The corresponding contributions to the total DOS are shown in the right panel.

filled bands originating from the minority spin t_{2g} orbitals of Fe_B cations. An energy gap of ~ 1 eV opens in the majority spin channel between occupied Fe_B e_g and the bottom of the empty Fe_A states. The lower part of the valence band (below -3.5 eV) is mainly formed by O $2p$ states with a bonding hybridization with Fe $3d$ states, whereas bands near the Fermi level, between -3.5 and 2 eV, have a predominant contribution of Fe $3d$ states.

It is worth recalling that Fe_B $3d$ states are split by the cubic component of a ligand field into a triplet t_{2g} and a doublet e_g. Already in the $Fd\bar{3}m$ phase the local symmetry of Fe_B sites ($D3d$) is lower than cubic and the trigonal component of the ligand field splits t_{2g} states into a singlet a_{1g} and doublet e'_g. In the monoclinic LT phase the symmetry is further lowered by the distortions and all the degeneracy is lifted. Nevertheless, the cubic component of the ligand field, which is determined by the relative strength of Fe $3d$–O $2p$ hybridization of π and σ type, remains dominant, whereas the splitting within t_{2g} and e_g subbands is smaller than the corresponding bandwidth. This allows one to label the corresponding states as t_{2g} and e_g. Note, however, that the $P2/c$ frame is rotated by $\sim \frac{\pi}{4}$ with respect to the $Fd\bar{3}m$ one and the angular dependence of the t_{2g} states is given by $d_{xz} \pm d_{yz}$ and $d_{x^2-y^2}$ combinations
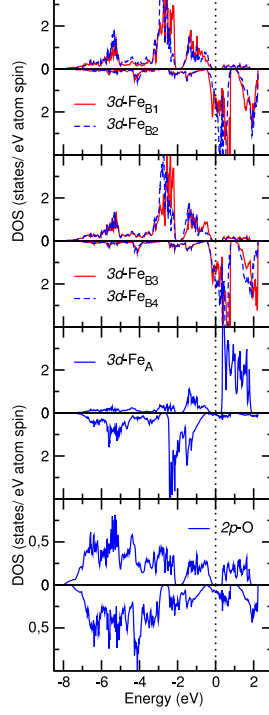
FIG. 2: (Color online) Partial DOS obtained from the LSDA calculations for the $P2/c$ phase of Fe_3O_4. The Fermi level is shown by dotted lines.

of cubic harmonics.

Figure 2 presents different contributions to the total density of states given by independent iron and oxygen sites. Crystallographically independent iron sites are labeled according to the notation of Ref. 11. Note, however, that the DOSs for two pairs of sites that were constrained to have equivalent coordination during the structural refinement – Fe_{B1a}, Fe_{B1b} and Fe_{B2a}, Fe_{B2b} – are very similar and we present the DOS averaged over the corresponding pairs, dropping a and b indices.

The splitting of Fe_B states due to the octahedral component of the ligand field is roughly of 1 eV. This is considerably smaller than the exchange splitting between minority and majority spin states, which is $\sim$3 eV, and consistent with the high-spin state of Fe cations. The absolute values of magnetic moments obtained by LSDA are $3.14\,\mu_B$, $3.30\,\mu_B$, $3.44\,\mu_B$, $3.27\,\mu_B$, and $3.38\,\mu_B$ for Fe_A and Fe_{B1-B4} cations, respectively. The total ferromagnetic moment per Fe_3O_4 formula unit is $4.0\,\mu_B$.

It should be noted that in contrast to experimental data the LSDA calculations result in a half-metallic solution without charge ordering. Apparently, the change of the LSDA

electronic structure, produced by the crystal structure distortion from the cubic to the mon-oclinic phase, is not sufficient to explain the charge ordering and metal-insulator transition in Fe_3O_4. The electron-electron correlations, mainly in the $3d$ shell of Fe cations, play a significant role.

V.   LSDA+U RESULTS

A.   Band structure

In order to account for the strong electronic correlations in the Fe $3d$ shell, at least on the static Hartree-Fock level, we calculated the electronic structure of the LT phase of Fe_3O_4 using the LSDA+U method. Previous studies proved this method to be quite successful in treating transition metal oxides with strong electron-electron correlations as well as systems with long-range order.[55,57,60,63] The value of the U parameter for Fe cations estimated using different experimental and theoretical technics lies in the range of 4.5-6 eV.[29,63,64] A reasonably good agreement of the calculated gap value of 0.18 eV with the experimental value[65] of 0.14 eV at 10 K was obtained using the U value of 5 eV. Note, however, that the charge and orbital order derived from the LSDA+U calculations does not depend on the exact U value when it is varied within the above mentioned limits. The value of the Hund's coupling J=1 eV was estimated from constrained LDA calculations.[66] In the following all results presented in the paper were obtained using a U value of 5 eV.

Figure 3 shows the LSDA+U band structure and the total DOS calculated self-consistently for the low-temperature structure of Fe_3O_4 using the Coulomb interaction parameter U=5 eV and exchange coupling J=1 eV. The corresponding partial Fe_B $3d$ DOS are shown in Fig. 4. The LSDA+U calculations give results qualitatively distinct from those of the LSDA. An indirect energy gap of 0.18 eV opens in the minority spin channel between M and Γ symmetry points. One of the minority spin t_{2g} states of Fe_{B1} and Fe_{B4} ions be-comes occupied while the Fe_{B2} and Fe_{B3} $t_{2g\downarrow}$ states are pushed above the chemical potential. Although, as will be discussed below, the calculated disproportion of Fe_B $3d$ charges is sig-nificantly less than 1, in the following we use the notations Fe^{2+} and Fe^{3+} for $Fe_{B1,B4}$ and $Fe_{B2,B4}$ cations, respectively, having in mind the difference of their t_{2g} occupations. The top of the valence band is formed by the occupied $t_{2g\downarrow}$ states of $B1$ and $B4$ Fe^{2+} cations.
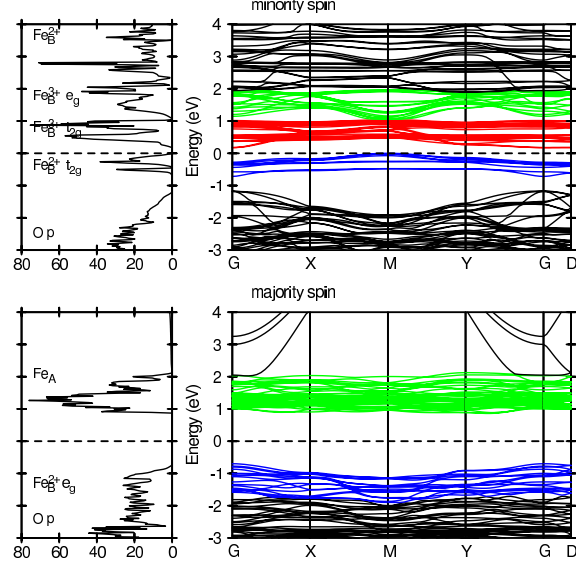
FIG. 3: (Color online) Total DOS and band structure of the $P2/c$ phase of Fe_3O_4 self-consistently obtained by the LSDA+U with U=5 eV and J=1 eV. The Fermi level is denoted by the horizontal line and is taken as the zero of energy. A band gap of 0.18 eV opens between M and Γ symmetry points. The energy bands predominantly originating from the Fe_B^{3+} t_{2g} and e_g states are shown in dark gray (red) and light gray (green) colors, respectively, whereas the gray (blue) color corresponds to Fe_B^{2+} t_{2g} bands. For the majority spin an energy gap of $\sim$2 eV opens between Fe_B^{2+} e_g and Fe_A bands shown in dark gray (red) and light gray (green) color, respectively. The corresponding contributions to the total DOS are shown in the left panel.

The bottom of the conduction band is formed predominantly by the empty $t_{2g\downarrow}$ states of $B2$ and $B3$ Fe^{3+} cations. The remaining unoccupied $t_{2g\downarrow}$ states of $B1$ and $B4$ Fe^{2+} cations are pushed by the strong Coulomb repulsion to energies above 2.5 eV. Majority spin $3d$ Fe_B states are shifted below O $2p$ states, which form a wide band in the energy interval between -7 and -2 eV. This is in strong contrast to the uniform half-metallic solution obtained by the LSDA.

Bands corresponding to the Fe_A^{3+} cations are fully occupied (empty) for minority (majority) spin states, respectively, and already in the LSDA do not participate in the formation of bands near the Fermi level. The LSDA+U method does not strongly affect these bands, which lie in the energy interval of -6 eV below and 1–2 eV above the Fermi level.
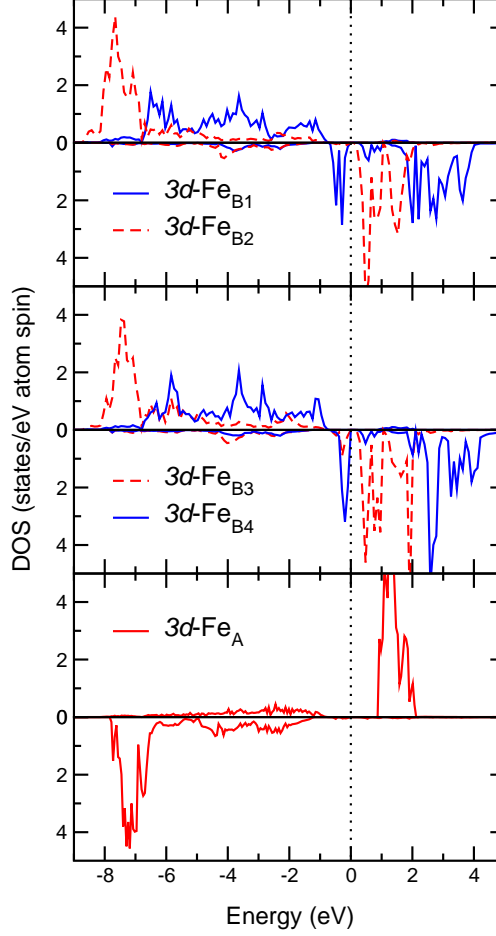
11

FIG. 4: (Color online) Partial DOS obtained from the LSDA+U calculations with U=5 eV and J=1 eV for the $P2/c$ phase of Fe_3O_4. The Fermi level shown by dotted lines. A charge-ordered insulating solution is obtained. Fe $3d$ minority states corresponding to $B1$ and $B4$ sites are occupied (Fe^{2+}) and located just below the Fermi level, whereas $B2$ and $B3$ are empty (Fe^{3+}). The charge difference between 2+ and 3+ Fe_B cations is found to be $0.23\,\bar{e}$.

B. Charge ordering

The obtained solution for CO of Fe^{2+} and Fe^{3+} cations on the B sublattice is described by a dominant $[001]_c$ charge (and spin) density wave, which originates from alternating chains of Fe^{2+} ions on octahedral $B1$ sites and Fe^{3+} ions on $B2$ sites (see Table I and Fig. 2 in Ref. 47). A secondary $[00\frac{1}{2}]_c$ modulation in the phase of CO, which is formed by the chain of alternately "occupied" Fe^{2+} ions on the $B4$ sites and "empty" Fe^{3+} ions on $B3$ sites, was found. This is consistent with a [001] nesting vector instability at the Fermi surface in the

Fe_B minority electron states which has been recently revealed by the LSDA calculations for the cubic phase.[62] The calculated CO scheme coincides with the class I CO model proposed by Wright *et al.*[11,45] All the tetrahedra formed by Fe_B cations have either a 3:1 or 1:3 ratio of Fe^{2+} and Fe^{3+} ions. Thus, the LSDA+U calculations confirm that the Anderson criterion is not satisfied in the LT phase. However, it should be pointed out that the Anderson criterion was introduced under the assumption of equal interatomic distances within each tetrahedron, whereas in the distorted LT structure the iron-iron distances vary from 2.86 to 3.05 Å. The same CO pattern has been recently confirmed by other LDA+U calculations.[48]

An analysis of the $3d$ minority occupation matrices of Fe_B cations confirms very effective charge disproportion within the Fe_B t_{2g} minority spin subshell. In particular, one of the $t_{2g\downarrow}$ states of Fe_{B1}^{2+} and Fe_{B4}^{2+} cations is almost completely filled with the occupation $n \approx 0.8$. On the other hand, the other two $t_{2g\downarrow}$ orbitals of the Fe_B^{2+} cations have significantly smaller population of about 0.04. The occupation numbers of $t_{2g\downarrow}$ orbitals for Fe_{B2}^{3+} and Fe_{B3}^{3+} cations do not exceed 0.1–0.17, which gives a value of about 0.7 for the largest difference of the populations of Fe_B^{2+} and Fe_B^{3+} $t_{2g\downarrow}$ states. The occupation numbers of the minority spin Fe_B $3d$ orbitals and the net occupations of the $t_{2g\downarrow}$ and $e_{g\downarrow}$ states are given in the last two columns of Table I.

The change of the $t_{2g\downarrow}$ occupations caused by the charge ordering is very effectively screened by the rearrangement of the other Fe electrons. A significant contribution to the screening charge is provided by Fe_B e_g states. Although the bands originating from these states are located well above the energy gap, the minority spin e_g orbitals form relatively strong σ bonds with $2p$ states of the oxygen octahedron and, as a result, give an appreciable contribution to the occupied part of the valence band. The energy of Fe_B^{3+} $e_{g\downarrow}$ states is lower than the energy of corresponding Fe_B^{2+} states and the former give a significantly larger contribution to the part of the valence band formed mainly by O $2p$ states. Because of the stronger covalency of the Fe_B^{3+} e_g- O p bonds the net occupation of Fe_B^{3+} $e_{g\downarrow}$ states becomes $\sim 0.25\,\bar{e}$ larger (see the last column of Table I). The resulting $3d$ charge difference (0.23) and disproportionation of the total electron charges inside the atomic spheres of Fe_B^{2+} and Fe_B^{3+} ions (0.24) are in reasonably good agreement with the value of 0.2 estimated from a BVS analysis of the $P2/c$ structure.[11,45] The above-mentioned screening of the changes in the Fe_B t_{2g} minority occupations reduces the energy loss due to the development of charge order incompatible with the Anderson criterion in the LT phase of Fe_3O_4.

Hence, due to the strong screening effects, the order parameter defined as the difference of the net $3d$ charges of Fe_B cations does not provide conclusive evidence for CO. This explains why the BVS analysis does not give a convincing proof of CO existence. Apparently, a well-defined order parameter is the difference of the occupations of the t_{2g} minority spin states for Fe_B^{3+} and Fe_B^{2+} cations which amounts to 70% of the ideal ionic CO model and clearly indicates the existence of a charge-ordered ground state below the Verwey transition.

The LSDA+U calculations were also performed for the assumption of Verwey charge order in the $P2/c$ structure. However, instead of the assumed Verwey CO the same self-consistent solution as the one described above was found. Therefore, the Verwey CO model is unstable in the distorted $P2/c$ structure. It is well known that with increasing U value localization is effectively increased. Remarkably, even for a U value increased up to 7–8 eV no Verwey-like CO pattern was found self-consistently in the distorted $P2/c$ structure. On the contrary, the LSDA+U calculations performed for an undistorted $P2/c$ supercell of the $Fd\bar{3}m$ structure result in an insulating CO solution which *is compatible* with the Verwey CO model. Altogether this implies that the Verwey CO model is unstable under a structure distortion from the high-symmetry cubic into the low-symmetry $P2/c$ phase.

Also we performed LSDA+U calculations with the same U and J parameters (5 and 1 eV, respectively) for the assumption of one of the 32 class II CO models within Cc supercell of $P2/c$, which is shown in Fig. 2 in Ref. 45. But we found that this kind of CO is unstable and the self-consistent solution coincides with the one found previously for the $P2/c$ structure.

Comparing the LSDA+U results for the undistorted and distorted $P2/c$ unit cells we can conclude that the charge-ordering pattern of Fe_B^{2+} and Fe_B^{3+} cations in the LT phase of Fe_3O_4, derived from the BVS analysis in Ref. 45 and confirmed by our study, *is mainly forced* by the local distortions of the crystal structure. Obviously we did not manage to study all possible charge- ordering scenarios within $P2/c$ or Cc supercell of $P2/c$. But our results consistently indicate the importance of the small amplitude of atomic displacements (almost of 0.07Å) recently resolved by x-ray and neutron powder diffraction.[11,45] The additional displacements leading to the Cc supercell were estimated to be of $\sim$0.01 Å but have not been fully resolved so far. They also may be important for full understanding of the CO in Fe_3O_4. In particular, in the $P2/c$ subcell the true atomic positions are averaged over the corresponding number of subsites in the Cc cell. Therefore, the actual arrangement of the locally Fe_BO_6 octahedra in the true Cc structure can be more complex, probably resulting in a more complicated

TABLE I: $3d$ orbital contribution to the formation of Fe$_B$ minority spin states with occupancy n evaluated by diagonalization of the occupation matrix. Although one of the $t_{2g\downarrow}$ states of $B1$ and $B4$ sites is almost occupied with $n \geq 0.7\,\bar{e}$ the t_{2g} minority spin occupancies of $B2$ and $B3$ Fe^{3+} cations are less than $0.1\,\bar{e}$. The occupied $t_{2g\downarrow}$ states of $B1$ and $B4$ Fe^{2+} cations are predominantly of $d_{xz} \pm d_{yz}$ and $d_{x^2-y^2}$ character, respectively. The sum of t_{2g} (e_g) occupations is given in the last column.

Fe$_B$ ion	sym.	t_{2g}			e_g		n	$\sum_{t_{2g}}$
		yz	zx	x^2-y^2	$3z^2-r^2$	xy		$(\sum_{e_g})$
Fe$_{B1a}$	t_{2g}	-0.47	-0.80	0.34	0.00	-0.07	0.81	0.89
		0.86	-0.33	0.40	-0.01	0.01	0.04	
		-0.21	0.49	0.84	-0.01	0.04	0.04	
	e_g	0.04	0.06	0.01	-0.49	-0.87	0.15	0.26
		-0.02	-0.03	-0.02	-0.87	0.48	0.11	
Fe$_{B1b}$	t_{2g}	-0.47	0.83	0.28	-0.03	0.12	0.71	0.79
		0.83	0.31	0.46	0.00	0.00	0.04	
		0.30	0.45	-0.84	0.00	0.02	0.04	
	e_g	-0.05	0.11	0.02	0.55	-0.83	0.15	0.27
		0.01	-0.04	0.00	0.83	0.55	0.12	
Fe$_{B2a}$	t_{2g}	0.00	0.91	0.41	0.00	0.00	0.09	0.24
		-0.99	0.00	0.01	0.00	0.00	0.08	
		-0.01	0.41	-0.91	-0.04	0.00	0.07	
	e_g	-0.01	0.00	0.00	0.00	0.99	0.27	0.52
		0.00	-0.02	0.04	-0.99	0.00	0.25	
Fe$_{B2b}$	t_{2g}	0.00	-0.90	0.45	0.01	0.00	0.09	0.23
		-0.99	-0.01	-0.03	0.00	-0.05	0.07	
		0.03	-0.45	-0.89	-0.04	0.00	0.07	
	e_g	0.00	-0.01	-0.04	0.99	0.00	0.26	0.52
		-0.05	0.00	0.00	0.00	0.99	0.26	
Fe$_{B3}$	t_{2g}	0.79	-0.18	0.53	-0.09	0.24	0.17	0.36
		-0.22	0.73	0.63	0.13	-0.10	0.11	
		0.52	0.65	-0.55	-0.08	-0.04	0.08	
	e_g	-0.21	0.12	0.04	-0.91	0.35	0.25	0.49
		0.13	-0.11	0.11	-0.39	-0.90	0.24	

charge and/or orbital order for the LT structure. The present calculations indicate that the competition of the "elastic" and electrostatic energy contributions in the total energy appears to be responsible for the CO, which is realized in the LT structure of Fe_3O_4.[47] Because of this, the Verwey CO model, which has the lowest electrostatic but significant "elastic" energy contribution in the total energy, becomes less favorable than other arrangements.

C.   Orbital ordering

The self-consistent solution obtained by the LSDA+U is not only charge but also orbitally ordered. It is clearly seen from Table I, which presents the contribution of $3d$ cubic harmonics to the formation of Fe_B minority spin states with an occupancy n (next to last column in Table I) evaluated by diagonalization of the corresponding occupation matrix self-consistently obtained by the LSDA+U.

As shown in the table the most occupied Fe^{2+} $3d$ minority orbitals are centered on the $B1a$, $B1b$, and $B4$ iron sites and have $d_{xz} - d_{yz}$, $d_{xz} + d_{yz}$, and $d_{x^2-y^2}$ character, respectively. Remarkably, the occupied $t_{2g\downarrow}$ orbitals of Fe_B cations are almost orthogonal to each other, i.e., their relative orientation corresponds to an anti-ferro-orbital order. Since all Fe_B cations are ferromagnetically coupled the obtained orbital order conforms with the anti-ferro-orbital ferromagnetic state, which is the ground state of the degenerate Hubbard model according to the Kugel-Khomskii theory.[67,68] This orbital order is consistent with the corresponding distortions of FeO_6 octahedra. In particular, using simple considerations which take into account only the change of the Fe-O bond lengths and neglect the bending of the bonds, it was previously concluded that the calculated orbital order is mainly determined by the distortions of oxygen octahedra surrounding Fe_B sites.[49]

Also this simple analysis shows a remarkable difference between Fe_{B1}^{2+} and Fe_{B4}^{2+} cations; namely, the average Fe_{B1a}-O distance in the plane of occupied $d_{xz} - d_{yz}$ orbital is 2.087 Å, whereas in the planes of two other t_{2g} orbitals they are only 2.063 and 2.067 Å. This difference between the average cation-anion distance in the planes of occupied and unoccupied orbitals is remarkably larger for $Fe_{B1a,b}$ (more than 0.02 Å), although for Fe_{B4} they are 2.074 and 2.067 Å for occupied $d_{x^2-y^2}$ and unoccupied $d_{xz} \pm d_{yz}$ orbitals, respectively, which gives a difference of only 0.007 Å. This small difference can be changed by applying a uniaxial stress to the $P2/c$ unit cell resulting in modification of the electronic properties.[69] In particular, a

few percent of magnitude elongation of the $P2/c$ unit cell along the c axis with simultaneous (in order to preserve the same unit cell volume) compression in the ab plane, gives rise to orbital-order crossover on the Fe$_{B4}$ site from a $d_{x^2-y^2}$ to a d_{xz} occupied orbital. At the same time the charge order and occupied orbitals on the Fe$^{2+}_{B1a,b}$ sites remain the same. The pressure-induced spatial reorientation of the occupied Fe$_{B4}$ t_{2g} orbital was proved by the LSDA+U calculations for the strained $P2/c$ unit cell. Note, however, that these rough estimations do not take into account the elastic anisotropy in Fe$_3$O$_4$. Moreover, the analysis was performed for the "averaged" $P2/c$ structure. However, they provide insight into the orbital-ordering phenomena behind the Verwey transition in magnetite as well as the problem of an external parameter-controlled electron state (for example, orbital ordering) in solids.[70]

D. Magnetic moments

The strong variation of the occupancies of the minority spin Fe$_B$ t_{2g} states leads to a pronounced modulation of the spin magnetic moments on the B sublattice. While the total moment per formula unit remains at $4\,\mu_B$ the magnetic moments of the Fe^{2+} $B1$ ($3.50\,\mu_B$) and $B4$ ($3.48\,\mu_B$) cations become appreciably smaller than Fe$_{B2}$ ($3.94\,\mu_B$) and Fe$_{B3}$ ($3.81\,\mu_B$) moments. The $[001]_c$ charge and spin modulation on the B sublattice is accompanied by formation of a weak spin modulation on the oxygen ions caused by different strengths of the hybridization of O $2p$ states with the minority spin $3d$ states of Fe$^{2+}_B$ and Fe$^{3+}_B$ ions. In particular, the oxygen magnetic moment reaches its maximal value of $\sim 0.1\,\mu_B$ for O3 and O4 ions, which lie in the plane of Fe$^{3+}_{B2}$ cations. It substantially decreases for other oxygen ions and approaches minimum for O1 and O2 lying in the plane of Fe$^{2+}_{B1}$ cations ($\sim 0.04\,\mu_B$).

Recently, an anomalously large value of the Fe$_B$ orbital magnetic moment reaching $0.33\,\mu_B$ has been deduced by applying sum rules to experimental $L_{2,3}$ x-ray magnetic circular dichroism spectra of Fe$_3$O$_4$.[71] In addition, the unquenched Fe$_B$ orbital moment was also reported to be confirmed by the LDA+U calculations. Later, however, this experimental finding was questioned by Goering *et al.*[72] The average orbital moments between $-0.001\,\mu_B$ and $0.06\,\mu_B$ were found from x-ray magnetic circular dichroism (XMCD) sum rules depending on the integration range. From our spin-polarized relativistic LSDA+U calculations for the LT structure we obtained the orbital moments of $0.19\,\mu_B$ and $0.014\,\mu_B$ for Fe$_{B1}$ and Fe$_{B2}$ ions. Somewhat larger values of $0.039\,\mu_B$ and $0.22\,\mu_B$ were calculated for Fe$_{B3}$ and Fe$_{B4}$ cations,

respectively. Taking into account the negative Fe_A orbital moment of $-0.021\,\mu_B$ this gives the value of $0.07\,\mu_B$ for the average orbital moment. Thus, in agreement with the previous theoretical results of Ref. 57 and XMCD sum rule data of Ref. 72, our calculations give the value of Fe orbital moment of $\sim 0.07\,\mu_B$ which is much smaller than reported in Ref. 71.
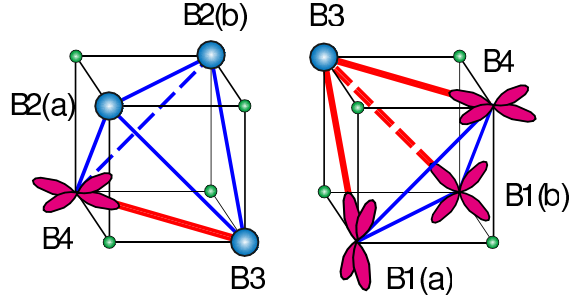
E. Exchange coupling constants

FIG. 5: (Color online) Sketch of the spatial arrangement of exchange interaction parameters between the octahedral Fe_B sites. Orbitals approximate the occupied $3d$ minority orbitals of Fe_B^{2+} cations. Fe_B^{3+} cations are shown by large (blue) spheres. Oxygen atoms are shown by small (green) spheres. Ferromagnetic couplings between Fe_B cations are shown by the thick (red) lines, whereas antiferromagnetic exchanges depicted by the thin (blue) lines.

To proceed further we performed calculations of the exchange interaction parameters J_{ij} via the variation of the ground state energy with respect to the magnetic moment rotation angle.[55] The exchange coupling parameter J_{ij} represents the effective pair exchange interaction between the ith and jth Fe atoms with effective Heisenberg Hamiltonian $H = -\sum_{i>j} J_{ij}\mathbf{S}_i \cdot \mathbf{S}_j$. Here, $\mathbf{S}_i$ and $\mathbf{S}_j$ are the spins at site i and j (5/2 and 2 for Fe^{3+} and Fe^{2+} cations, respectively). Positive (negative) values of J_{ij} correspond to the ferromagnetic (antiferromagnetic) coupling between sites. As shown in Table II the exchange couplings between A and B iron sublattices are rather large, of about -70 K, and antiferromagnetic. The Fe_A–Fe_A interactions are weakly antiferromagnetic with the maximal absolute value of 9.3 K (not shown in Table II). The exchange couplings between the Fe_B sites ($|J_{BB}| \leq 27.5$ K) are substantially smaller than Fe_A–Fe_B ones and almost all of them are ferromagnetic (see Fig. 5). Weak antiferromagnetic couplings with $|J_{BB}| \leq 11.6$ K are also obtained [mainly between the sites with the same 2+ or 3+ valence state, shown by the thin (blue) lines in

TABLE II: Exchange couplings J_{ij} (all with $|J_{ij}| > 10$ K) are presented. The values are given in kelvin. The spatial representation of the Fe_B–Fe_B exchange couplings is schematically shown in Fig. 5. J_{ij} were calculated between the sublattices formed by the translations of the following Fe sites: Fe_{A1} (1/4,0.0034,0.06366), Fe_{A2} (1/4,−0.4938,0.18867), Fe_{B1a} (0,1/2,0), Fe_{B1b} (1/2,1/2,0), Fe_{B2a} (0,0.0096,1/4), Fe_{B2b} (1/2,0.0096,1/4), Fe_{B3} (−1/4,0.2659,0.1198), Fe'_{B3} (1/4,−0.2659,−0.1198), Fe''_{B3} (1/4,0.2659,0.3801), Fe_{B4} (1/4,0.2479,−0.1234), Fe'_{B4} (−1/4,−0.2479,0.1234), and Fe''_{B4} (1/4,−0.2479,0.3765).

i-atom	j-atom	J_{ij}, K
Fe_{A1}	Fe_{B1a}	−69.7
	Fe_{B1b}	−69.9
	Fe_{B2a}	−42.0
	Fe_{B2b}	−42.1
	Fe_{B3}	−73.7
	Fe'_{B3}	−48.1
	Fe_{B4}	−39.2
	Fe'_{B4}	−52.9
Fe_{A2}	Fe_{B1a}	−40.0
	Fe_{B1b}	−27.0
	Fe_{B2a}	−74.8
	Fe_{B2b}	−77.4
	Fe_{B3}	−89.1
	Fe''_{B3}	−31.1
	Fe'_{B4}	−62.7
	Fe''_{B4}	−27.8
Fe_{B1a}	Fe_{B3}, Fe'_{B3}	+12.7
Fe_{B1b}	Fe_{B3}, Fe'_{B3}	+27.5
Fe_{B2a}	Fe_{B2b}	−11.6
Fe_{B3}	Fe'_{B4}	+16.8
Fe_{B4}	Fe'_{B3}	+16.8
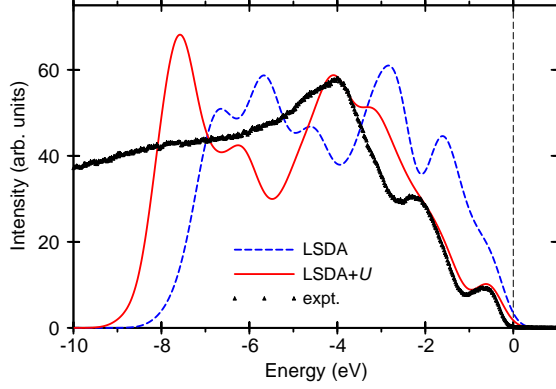
FIG. 6: (Color online) Comparison of the total DOS obtained from LSDA (dashed line) and LSDA+U calculations with U=5 eV and J=1 eV (solid line) to the experimental XPS spectrum taken from Ref. 36 (triangles). A rigid shift of -0.3 eV is applied to the calculated DOS curves.

Fig. 5]. The spatial representation of these exchange couplings is presented in Fig. 5. Other couplings that are not shown in Table II are weaker than 10 K.

Experimental estimation of the exchange couplings in Fe_3O_4 was first performed by Néel on the basis of the two-sublattice collinear model.[73] From analysis of the temperature behaviour of the saturation magnetization and paramagnetic susceptibility he obtained $J_{AA} = -17.7$, $J_{AB} = -23.4$, and $J_{BB} = 0.5$ K, where A and B refer to the tetrahedral and octahedral Fe sites, respectively. We find these values qualitatively in accord with our results presented in Table II; namely, as in Néel's model, the calculations result in strong antiferromagnetic coupling between the A and B sublattices; J_{AA} couplings (not shown in Table II) are considerably smaller than J_{AB}; the exchange couplings in the B sublattice are weak and almost all of them are ferromagnetic. On the other hand, the small antiferromagnetic Fe_{B2a}^{3+}–Fe_{B2b}^{3+} exchange interaction (see Table II) is in exact agreement with recent estimations using the two-sublattice model.[74] Three-sublattice model calculations give an overall similar result, except, however, the Fe_B^{2+}–Fe_B^{2+} exchange coupling, which seems to be overestimated.[75]

20

VI. SPECTRAL PROPERTIES

A. XPS spectra

In Fig. 6 the LSDA and LSDA+U total DOSs are compared to the soft x-ray photoemission (XPS) spectrum from Ref. 36. No attempts to account for different cross sections of Fe $3d$ and O $2p$ states have been made. To account for the experimental resolution and finite lifetime broadening the theoretical spectrum was convoluted with a Gaussian with a half-width of 0.4 eV. The calculated DOS curves had to be shifted by 0.3 eV to lower energies in order to align the experimental peak at ~ -0.7 eV with the corresponding peak in the LSDA+U DOS. The necessity of the rigid shift can be attributed to the problem of experimental determination of the Fermi level position for insulating samples. A similar shift of 0.2 eV was used in Ref. 76 when comparing photoelectron spectra to LSDA calculations. The experimental spectrum was measured at 100 K using Fe $2p$–$3d$ resonance photoemission with the photon energy $h\nu = 707.6$ eV. Because of the the relatively large escape depth of photoelectrons at this photon energy it is expected that the spectrum mainly probes bulk electronic states of Fe_3O_4.

Figure 6 shows that the shift of the position of the occupied majority spin Fe_B and minority spin Fe_A states to lower energies in the LSDA+U calculation greatly improves the agreement with the experiment. A feature at ~ -0.7 eV, which transforms to a well defined peak in the LSDA+U calculations, can be identified as $d^6 \rightarrow d^5$ transitions at Fe_B^{2+} ions. This peak is completely spin polarized in accordance with the finding of a recent spin-resolved photoemission study.[77] From a comparison with the l-projected DOS shown in Fig. 4 one can associate an experimental peak at 2 eV with transitions from the majority spin Fe_B^{2+} e_g states which give the predominant contribution in this energy range. In the calculated DOS, however, this feature is masked by a peak at ~ -3 eV and appears only as a shoulder. A peak at 4 eV in the experimental spectrum originates to a great extent from the transitions from the majority spin Fe_B^{2+} t_{2g} strongly hybridized with O $2p$ states. Note, however, that $3d$ states of other Fe ions as well as O $2p$ states also contribute to the total DOS in the energy range from -7 to -4 eV. Finally, a DOS peak at -7.8 eV formed mainly by the majority spin Fe_B^{3+} and minority spin Fe_A $3d$ states accounts for a weak feature found at -8 eV in the experimental spectrum. This feature seems to be masked by a high-energy satellite but

can be clearly seen in Fe $3p$–$3d$ resonance photoemission ($h\nu = 56$ eV).[76]

B.   Optical and magneto-optical spectra

Motivated by the fact that previous calculations were performed for the undistorted *cubic* structure assuming the Verwey CO pattern,[57] in this section we present the optical and magneto-optical spectra calculated for the $P2/c$ structural model of the LT phase of Fe$_3$O$_4$. Figure 7 shows optical conductivity (top) and reflectivity (bottom) calculated using the LSDA and LSDA+U with U=5 eV and J=1 eV. Symmetry lowering from the fcc to $P2/c$ structure causes some degree of optical anisotropy in the low-frequency range. However, it is rather weak and here we present the spectra averaged over different photon polarizations. The results are compared to the experimental optical spectra taken from Ref. 65, which reveal strong temperature dependence only in the narrow energy range of 0–1 eV.

The LT structure distortions have a rather weak effect on the LSDA spectra which resemble closely the spectra calculated for the cubic phase.[57] This finding agrees well with the fact that the LSDA band structure presented above is not strongly affected by the crystal structure distortions. It is worth recalling that the LSDA calculations result in a metallic solution and therefore give the wrong asymptotic behavior for the optical reflectivity at $\omega \to 0$. Moreover, a peak at ∼6.5 eV in the calculated conductivity spectrum is shifted to higher energies with respect to the experimental peak centered at ∼5 eV. Both conductivity and reflectivity show peaks at 2 eV which are much higher than in the experimental spectra. Hence, the LSDA theory fails to correctly reproduce the low-energy spectral properties of Fe$_3$O$_4$, whereas it describes reasonably well the experimental spectra above 10 eV.

As in Ref. 57 better agreement between the calculated and experimental spectra was obtained using the LSDA+U method. Since the self-consistent LSDA+U solution is insulating the reflectivity at zero frequency is no longer equal to 1 but approaches the value of 0.6 which, however, is somewhat higher than in the experiment. Figure 8 shows the expanded view of the theoretical and experimental[65] optical spectra in a smaller frequency range below 8 eV. Charge and orbital ordering within the minority spin Fe$_B$ t_{2g} states changes drastically the spectrum below 3 eV. Because of the shift of the unoccupied minority spin Fe$_B^{2+}$ and majority spin Fe$_A$ d states to higher energies as compared to their LSDA positions the spectral weight is transferred from 2 eV to higher frequencies. This improves the agreement
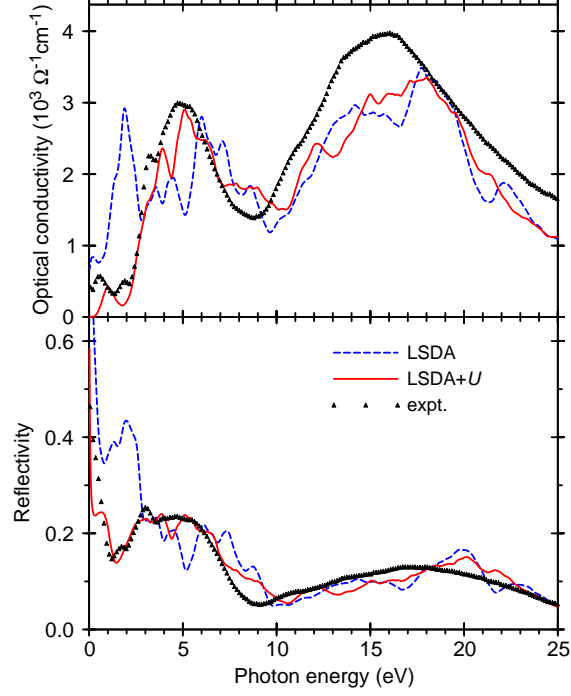
FIG. 7: (Color online) Reflectivity (lower panel) and optical conductivity (upper panel) spectra calculated using the LSDA (dashed line) and LSDA+U with U=5 eV and J=1 eV (solid line) for the $P2/c$ model of the LT phase of Fe_3O_4. Room temperature experimental spectra from Ref. 65 are shown by triangles.
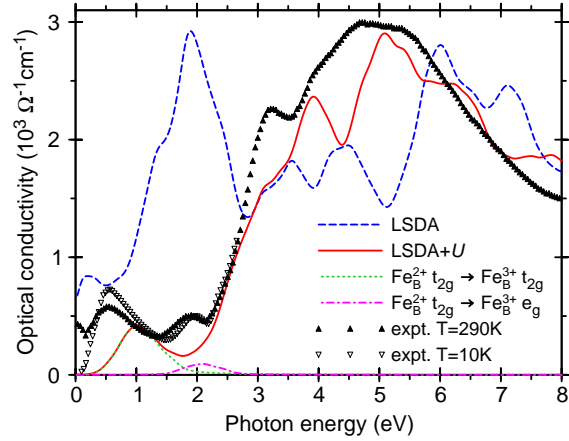

FIG. 8: (Color online) Comparison of LSDA (dashed line) and LSDA+U with U=5 eV and J=1 eV (solid line) optical conductivity spectra to the experimental spectra measured at room temperature (up triangles) and at 10 K (down triangles).[65] Also plotted are the contributions of the interband transitions from occupied minority spin Fe_B^{2+} t_{2g} to Fe_B^{3+} t_{2g} (short-dashed line) and Fe_B^{3+} e_g (dash-dotted line) to the LSDA+U spectrum.

with the experimental optical conductivity in the range 3.5–6 eV. However, instead of the two-peak structure at 0.5 and 2 eV the LSDA+U calculations reveal a maximum at $\sim$1 eV which can be associated with the 0.5 eV peak in the experimental spectrum. The theoretical peak is, however, more symmetric, shifted to higher frequencies, and its magnitude is lower than in the experiment. An analysis of different interband contributions to the calculated spectra shows that the 1 eV peak is predominantly formed by the transitions from occupied Fe_B^{2+} $t_{2g\downarrow}$ into empty Fe_B^{3+} $t_{2g\downarrow}$ bands. The maximum of the Fe_B^{2+} $t_{2g\downarrow}$ to Fe_B^{3+} $e_{g\downarrow}$ interband conductivity coincides with the second experimental peak at $\sim$2 eV. However, its theoretical intensity is too low and these transitions do not manifest themselves as a peak in the spectrum.

An attempt to make the agreement between the theoretical and experimental spectra better by decreasing the value of U has not given any substantial improvements. In particular for U=4.5 eV (not shown here) the 1 eV peak shifts to lower energies only by 0.2 eV. Moreover, its shape is still more symmetric than the shape of the corresponding peak in the experimental spectra at 10 K,[65] whereas the theoretical intensity of the second peak remains too low.

A possible reason for the abovementioned discrepancies between the theoretical and experimental spectra below 2 eV can be neglecting dynamical correlations in the frame of the static LSDA+U method. Moreover, it is worth recalling that the true LT crystal structure has not been fully resolved yet and the calculations were performed for the "averaged" $P2/c$ structural model for the LT phase of Fe_3O_4. As described in Sec. V B the self-consistently obtained CO corresponds to the class I CO model.[45] If one of the class II CO patterns is realized in the true Cc structure, as has been suggested by a recent resonant x-ray diffraction study,[78] then more complicated charge and orbital order may result in narrowing of Fe_B d-derived bands and a shift of the peak in optical absorption to lower energies. Therefore, further investigations of the LT crystal structure are strongly demanded.

In Fig. 9 magneto-optical polar Kerr rotation and ellipticity spectra calculated for the $P2/c$ structural model are compared to the room temperature spectra of the annealed synthetic sample of Fe_3O_4.[79] Calculations were performed assuming that the magnetization and light propagation directions are parallel to the c axis of the $P/2c$ cell. Similar to the optical conductivity spectra the use of the LSDA+U approach improves the agreement with the experiment above 2 eV. The minimum at 1.3 eV in the theoretical Kerr rotation spectrum is,
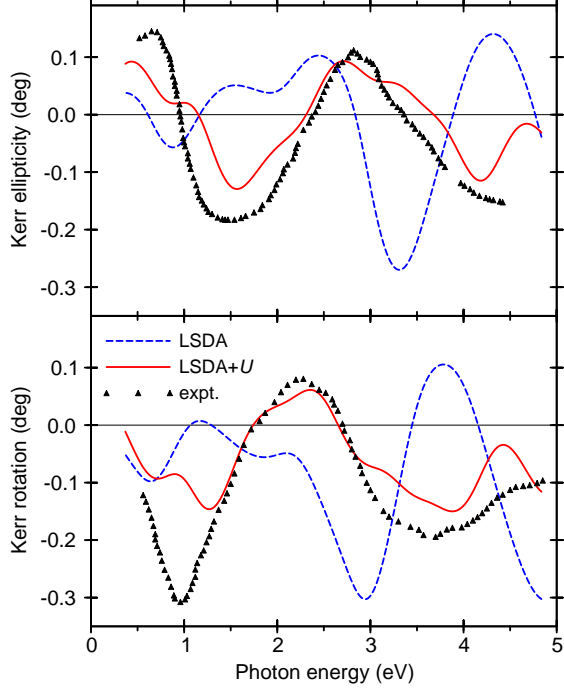
FIG. 9: (Color online) Polar Kerr rotation (lower panel) and ellipticity (upper panel) calculated for the $P2/c$ model of the LT phase of Fe_3O_4 using LSDA (dashed line) and LSDA+U with $U=5$ eV and $J=1$ eV (solid line). Experimental spectra measured at room temperature for an annealed synthetic sample of Fe_3O_4 in Ref. 79 are plotted by triangles.

however, less pronounced and shifted to higher frequencies as compared to the experimental one (measured at room temperature). Comparison of the magneto-optical spectra for the LT phase to the spectra calculated assuming the Verwey CO in the fcc unit cell[57] shows that the theoretical spectra are rather sensitive to the structural and CO model used in the calculations. Its experimental measurements for the LT phase of Fe_3O_4 and comparison with the theoretical prediction presented in Fig. 9 are of strong importance.

C.   O K-edge XAS

In the process of x-ray absorption at the O K edge a core O $1s$ electron is excited into unoccupied states in the conduction band. In the dipole approximation, which was used in the present calculations, the final states for the transition are of p symmetry and the spectrum probes the density of unoccupied O $2p$ states. O K-edge x-ray absorption spectra calculated using the LSDA and LSDA+U (with $U=5$ eV and $J=1$ eV) and averaged over
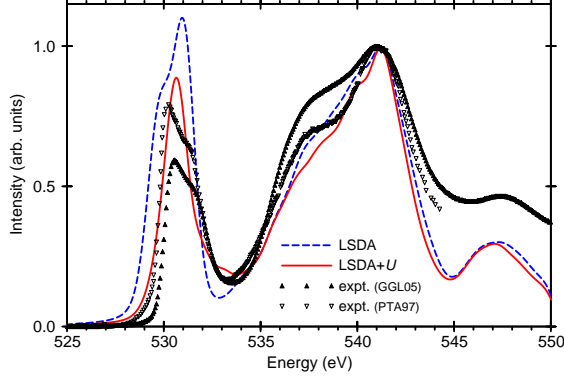
FIG. 10: (Color online) LSDA (dashed line) and LSDA+U with U=5 eV and J=1 eV (solid line) O K-edge x-ray absorption spectra calculated for the $P2/c$ model of the LT phase of Fe_3O_4. The sum of the spectra from inequivalent O sites is shown. Experimental spectra from Refs. 35 and 80 are plotted by down and up triangles, respectively.

eight inequivalent O sites in the $P2/c$ unit cell are presented in Fig. 10. Experimental spectra taken from Refs. 35 and 80 are shown in Fig. 10 by down and up triangles, respectively. In order to account for the effect of the final life time of the O $1s$ core hole and experimental resolution the spectra were broadened by convolution with Lorentzian and Gaussian functions of the width of 0.4 and of 0.5 eV, respectively. Then the calculated spectra were aligned and normalized to the main absorption peak at 541 eV in the experimental spectrum.

As mentioned in Sec. IV the lattice distortions themselves have only a weak effect on the LSDA band structure of Fe_3O_4 and the LSDA spectra calculated for inequivalent O sites in the $P2/c$ cell resemble closely the O K-edge spectrum for the undistorted $Fd\bar{3}m$ structure. Both the LSDA and LSDA+U spectra reproduce well the shape of the 541 eV peak and the position of a peak at 547.5 eV. Our calculations confirm the conclusion of Ref. 81 that these peaks originate from transitions to bands formed mainly by delocalized Fe $4s$ and $4p$ states.

The so-called preedge peak at 531 eV is formed by transitions to O $2p$ states hybridized with Fe_A and Fe_B $3d$ states and, thus, is more sensitive to the changes of the electronic structure caused by charge and orbital ordering effects. The preedge peak in the LSDA spectrum is wider than the experimental one, more intense, and shifted to lower energies. The experimental peak exhibits a second feature that appears as a shoulder at the high-energy slope of the peak. The LSDA spectrum also has a two-feature structure but their intensities are reversed. The two-feature structure of the preedge peak was interpreted as

coming from the hybridization of O $2p$ states with Fe $3d$ states split by the ligand field.[81] Indeed, the comparison of the O K-edge spectrum calculated for the undistorted fcc structure to the corresponding DOS shows that the low-energy shoulder is formed by transitions to O $2p$ states hybridized with majority spin Fe$_A$ $3d$ states of e symmetry and minority spin Fe$_B$ t_{2g} states, whereas the main peak reflects the O $2p$ hybridization with Fe$_A$ $t_{2\uparrow}$ and Fe$_B$ $e_{g\downarrow}$ states. In the latter case the O $2p$ – Fe $3d$ hybridization is stronger and this causes the higher intensity of the corresponding feature in the LSDA spectrum. It should be noted that calculations of the O K-edge spectrum based on the multiple-scattering approach reproduced the relative intensities of the two features of the preedge peak.[81]

O K-edge spectra calculated for inequivalent O sites in the $P2/c$ unit cell using the LSDA+U approach show much stronger variation of the shape of the preedge peak as compared to the LSDA calculations. The strongest deviation of the peak shape is found for those O ions that have only Fe$_B^{2+}$ cations among their nearest neighbors. In spite of that, the preedge peak in the averaged spectrum becomes narrower than the LSDA one and shifts to higher energies. An additional feature does appear at the high-energy slope of the peak but its intensity is much weaker than in the experiment.

We can conclude that LSDA+U calculations reproduce better the energy position of the preedge peak in the O K-edge spectrum but the shape of the peak still differs from the experimentally observed one. Calculations performed for other CO models possible in the true Cc structure might in principle improve the agreement with the experiment. We have to note, however, that recent measurements of the O K-edge spectrum performed in a wide temperature range below and above the Verwey transition show very small variation of the shape of the preedge peak.[80] This implies that the O K-edge spectrum should not be very sensitive to the details of a particular CO pattern. Many-body effects that are beyond the LSDA+U may be responsible for the disagreement between the theory and the experiment.

VII. SUMMARY AND CONCLUSIONS

In summary, in the present LSDA+U study of the $P2/c$ model of the LT phase of Fe$_3$O$_4$ we found a charge- and orbitally ordered insulator with an energy gap of 0.18 eV. The obtained charge-ordered ground state is described by a dominant $[001]_c$ charge density wave with a minor $[00\frac{1}{2}]_c$ modulation on the Fe$_B$ sublattice. A weak $[001]_c$ spin/charge modulation

27

on the oxygen ions was also obtained. The CO coincides with the earlier proposed class I CO[11,45] and confirms violation of the Anderson criterion.[18] While the screening of the charge disproportion is so effective that the total $3d$ charge disproportion is rather small (0.23), the charge order is well pronounced with an order parameter defined as the difference of $t_{2g\downarrow}$ occupancies of 2+ and 3+ Fe_B cations (0.7). This agrees well with the result of BVS analysis for a monoclinic structure (0.2). The orbital order is in agreement with the Kugel-Khomskii theory[67] and corresponds to the local distortions of oxygen octahedra surrounding Fe_B sites. The average Fe orbital moment of $\sim 0.07\,\mu_B$ agrees well with the recent experimental findings.[82]

Calculations of the effective exchange coupling constants between Fe spin magnetic moments show that the dominating interaction is an antiferromagnetic coupling between Fe_A and Fe_B moments. The coupling between Fe_B^{2+} and Fe_B^{3+} moments is found to be weaker and ferromagnetic.

The relevance of the charge-ordered LSDA+U solution has been verified by performing calculations of optical, magneto-optical polar Kerr rotation, and O K-edge x-ray absorption spectra and comparing them to available experimental data. The LSDA+U spectra show much better agreement with the experimental ones as compared to the spectra calculated for the charge-uniform LSDA solution. Unfortunately, the remaining discrepancies between the theory and the experiment in the low-frequency part of the optical and MO spectra and in the shape of the preedge peak in x-ray absorption do not allow us to discriminate among different CO models in the true Cc structure.

[1] J. H. de Boer and E. J. W. Verwey, Proc. Phys. Soc. London Sec. A **49**, 59 (1937).

[2] R. Peierls, Proc. Phys. Soc. London Sec. A **49**, 72 (1937).

[3] F. Bloch, Z. Phys. **57**, 545 (1929).

[4] A. Sommerfeld, Z. Phys. **47**, 1 (1928).

[5] A. H. Wilson, Proc. R. Soc. London, Ser. A **133**, 458 (1931).

[6] A. H. Wilson, Proc. R. Soc. London, Ser. A **134**, 277 (1931).

[7] M. Imada, A. Fujimori, and Y. Tokura, Rev. Mod. Phys. **70**, 1039 (1998).

[8] E. J. W. Verwey, Nature (London) **144**, 327 (1939).

[9] E. J. Verwey and P. Haayman, Physica (Amsterdam) **8**, 1979 (1941).

[10] E. J. W. Verwey, P. W. Haayman, and F. C. Romeijan, J. Chem. Phys. **15**, 181 (1947).

[11] J. P. Wright, J. P. Attfield, and P. G. Radaelli, Phys. Rev. Lett. **87**, 266401 (2001).

[12] G. Subías, J. García, J. Blasco, M. G. Proietti, H. Renevier, and M. C. Sánchez, Phys. Rev. Lett. **93**, 156408 (2004).

[13] D. C. Mattis, *The Theory of Magnetism I* (Springer, Berlin, 1988).

[14] K. Renger, "Die anfängliche Suszeptibilität von Eisen und Magnetit in Abhängigkeit von der Temperatur", Thesis, Zürich (1913).

[15] P. Weiss and K. Renger, Arch. Elektrotech. (Berlin) **11**, 406 (1914).

[16] T. Okamura, Sci. rep. Tohoku Imp. Univ. **21**, 231 (1932).

[17] B. S. Ellefson and N. W. Taylor, J. Chem. Phys. **2**, 58 (1934).

[18] P. W. Anderson, Phys. Rev. **102**, 1008 (1956).

[19] N. C. Tombs and H. P. Rooksby, Acta Crystallogr. **4**, 474 (1951).

[20] H. P. Rooksby and B. T. M. Willis, Acta Crystallogr. **6**, 565 (1953).

[21] E. J. Samuelsen, E. J. Bleeker, L. Dobrzynski, and T. Riste, J. Appl. Phys. **39**, 1114 (1968).

[22] T. Yamada, K. Suzuki, and S. Chikazumi, Appl. Phys. Lett. **13**, 172 (1968).

[23] J. Yoshida and S. Iida, J. Phys. Soc. Jpn. **47**, 1627 (1979).

[24] Y. Miyamoto and M. Shindo, J. Phys. Soc. Jpn. **62**, 1423 (1993).

[25] Several reviews of research on the Verwey transition up to 1980 are contained in the special issue of Philos. Mag. B **42** (1980).

[26] J. R. Cullen and E. R. Callen, Phys. Rev. Lett. **26**, 236 (1971).

[27] J. R. Cullen and E. R. Callen, Phys. Rev. B **7**, 397 (1973).

[28] M. Mizoguchi, J. Phys. Soc. Jpn. **44**, 1501 (1978).

[29] J. M. Zuo, J. C. H. Spence, and W. Petuskey, Phys. Rev. B **42**, 8451 (1990).

[30] N. F. Mott, Philos. Mag. B **42**, 327 (1980).

[31] Y. Yamada, Philos. Mag. B **42**, 377 (1980).

[32] D. Ihle and B. Lorenz, J. Phys. C **19**, 5239 (1986).

[33] H. Seo, M. Ogata, and H. Fukuyama, Phys. Rev. B **65**, 085107 (2002).

[34] A. Chainani, T. Yokoya, T. Morimoto, T. Takahashi, and S. Todo, Phys. Rev. B **51**, 17976 (1995).

[35] J.-H. Park, L. H. Tjeng, J. W. Allen, P. Metcalf, and C. T. Chen, Phys. Rev. B **55**, 12813 (1997).

[36] D. Schrupp, M. Sing, M. Tsunekawa, H. Fujiwara, S. Kasai, A. Sekiyama, S. Suga, T. Muro, V. A. M. Brabers, and R. Claessen, Europhys. Lett. **70**, 789 (2005).

[37] A. Pimenov, S. Tachos, T. Rudolf, A. Loidl, D. Schrupp, M. Sing, R. Claessen, and V. A. M. Brabers, Phys. Rev. B **72**, 035131 (2005).

[38] P. Weiss and R. Forrer, Ann. Phys. **12**, 279 (1929).

[39] V. C. Rakhecha and N. S. Murthy, J. Phys. C: Solid State Phys. **11**, 4389 (1978).

[40] Y. S. Dedkov, U. Rüdiger, and G. Güntherodt, Phys. Rev. B **65**, 064417 (2002).

[41] M. Fonin, R. Pentcheva, Y. S. Dedkov, M. Sperlich, D. V. Vyalikh, M. Scheffler, U. Rüdiger, and G. Güntherodt, Phys. Rev. B **72**, 104436 (2005).

[42] R. Pentcheva, F. Wendler, H. L. Meyerheim, W. Moritz, N. Jedrecy, and M. Scheffler, Phys. Rev. Lett. **94**, 126101 (2005).

[43] V. Y. Irkhin, M. I. Katsnelson, and A. I. Lichtenstein, *Lecture Notes in Physics*, edited by M. Donath and W. Nolting (Springer, 2005), Vol. 678, pp. 217–243.

[44] N. E. Brese and M. O'Keeffe, Acta Crystallogr. Sect. B **47**, 192 (1991).

[45] J. P. Wright, J. P. Attfield, and P. G. Radaelli, Phys. Rev. B **66**, 214422 (2002).

[46] J. Garcia, G. Subias, J. Blasco, and M. G. Proietti, cond-mat/0211407 (unpublished).

[47] I. Leonov, A. N. Yaresko, V. N. Antonov, M. A. Korotin, and V. I. Anisimov, Phys. Rev. Lett. **93**, 146404 (2004).

[48] H. T. Jeng, G. Y. Guo, and D. J. Huang, Phys. Rev. Lett. **93**, 156403 (2004).

[49] I. Leonov, A. N. Yaresko, V. N. Antonov, J. P. Attfield, and V. I. Anisimov, Phys. Rev. B **72**, 014407 (2005).

[50] I. Leonov, A. N. Yaresko, V. N. Antonov, U. Schwingenschlögl, V. Eyert, and V. I. Anisimov, cond-mat/0508378 (unpublished).

[51] A. Yaresko, I. Leonov, and P. Fulde, Physica B **378-380**, 1054 (2006).

[52] I. Leonov, "Charge order in transition metal oxides", Thesis, Universität Augsburg, Augsburg (2006).

[53] M. Iizumi, T. F. Koetzle, G. Shirane, S. Chikazumi, M. Matsui, and S. Todo, Acta Cryst. **B38**, 2121 (1982).

[54] V. I. Anisimov, J. Zaanen, and O. K. Andersen, Phys. Rev. B **44**, 943 (1991).

[55] A. I. Liechtenstein, V. I. Anisimov, and J. Zaanen, Phys. Rev. B **52**, R5467 (1995).

[56] O. K. Andersen, Phys. Rev. B **12**, 3060 (1975).

[57] V. N. Antonov, B. N. Harmon, V. P. Antropov, A. Y. Perlov, and A. N. Yaresko, Phys. Rev. B **64**, 134410 (2001).

[58] A. Perlov, A. Yaresko, and V. Antonov, *PY-LMTO, A Spin-polarized Relativistic Linear Muffin-tin Orbitals Package for Electronic Structure Calculations*, unpublished.

[59] V. Antonov, B. Harmon, and A. Yaresko, *Electronic structure and magneto-optical properties of solids* (Kluwer Academic Publishers, Dordrecht, Boston, London, 2004).

[60] V. N. Antonov, B. N. Harmon, and A. N. Yaresko, Phys. Rev. B **67**, 024417 (2003).

[61] Z. Zhang and S. Satpathy, Phys. Rev. B **44**, 13319 (1991).

[62] A. Yanase and N. Hamada, J. Phys. Soc. Jpn. **68**, 1607 (1999).

[63] V. I. Anisimov, I. S. Elfimov, N. Hamada, and K. Terakura, Phys. Rev. B **54**, 4387 (1996).

[64] J. Chen, D. J. Huang, A. Tanaka, C. F. Chang, S. C. Chung, W. B. Wu, and C. T. Chen, Phys. Rev. B **69**, 085107 (2004).

[65] S. K. Park, T. Ishikawa, and Y. Tokura, Phys. Rev. B **58**, 3717 (1998).

[66] W. E. Pickett, S. C. Erwin, and E. C. Ethridge, Phys. Rev. B **58**, 1201 (1998).

[67] K. I. Kugel and D. I. Khomskii, Sov. Phys. Solid State **17**, 285 (1975).

[68] K. I. Kugel and D. I. Khomskii, Sov. Phys. Usp. **25**, 231 (1982).

[69] H. Häffner, "Untersuchung des Verwey-Übergangs in Magnetit unter uniaxialem Druck", Diplomarbeit, Universität Augsburg, Augsburg (2003).

[70] I. Loa, X. Wang, K. Syassen, H. Roth, T. Lorenz, M. Hanfland, and Y.-L. Mathis, cond-mat/0504383 (unpublished).

[71] D. J. Huang, C. F. Chang, H. T. Jeng, G. Y. Guo, H. J. Lin, W. B. Wu, H. C. Ku, A. Fujimori, Y. Takahashi, and C. T. Chen, Phys. Rev. Lett. **93**, 077204 (2004).

[72] E. Goering, S. Gold, M. Lafkioti, and G. Schutz, Europhys. Lett. **73**, 97 (2006).

[73] L. Néel, Ann. Phys. (Paris) **3**, 137 (1948).

[74] J. Loos and P. Novák, Phys. Rev. B **66**, 132403 (2002).

[75] C. M. Srivastava, G. Srinivasan, and N. G. Nanadikar, Phys. Rev. B **19**, 499 (1979).

[76] Y. Q. Cai, M. Ritter, W. Weiss, and A. M. Bradshaw, Phys. Rev. B **58**, 5043 (1998).

[77] D. Huang, C. Chang, J. Chen, L. Tjeng, A. Rata, W. Wu, S. Chung, H. Lin, T. Hibma, and C. Chen, J. Magn. Magn. Mater. **239**, 261 (2002).

[78] R. J. Goff, J. P. Wright, J. P. Attfield, and P. G. Radaelli, J. Phys.: Condens. Matter **17**, 7633 (2005).

[79] X. Zhang, J. Schoenes, and P. Wachter, Solid State Commun. **39**, 189 (1981).

[80] E. Goering, S. Gold, M. Lafkioti, G. Schütz, and V. A. M. Brabers, Phys. Rev. B **72**, 033112 (2005).

[81] Z. Y. Wu, S. Gota, F. Jollet, M. Pollak, M. Gautier-Soyer, and C. R. Natoli, Phys. Rev. B **55**, 2570 (1997).

[82] E. Goering, M. Lafkioti, and S. Gold, Phys. Rev. Lett. **96**, 039701 (2006).